Theory, Modeling and
Luminescence Phenomena

Electronic Structures and Nature of Host Excitation in Gallates

P. C. Schmidt[+], J. Sticht[+], M. Stephan[+], V. Eyert[++] and K. C. Mishra[*]
[+] Institut für Physikalische Chemie,Technische Universität Darmstadt, Darmstadt, Germany
[++] Institut für Physik, Universität Augsburg, Augsburg, Germany
[*] Research and Development, OSRAM SYLVANIA, Beverly, MA

Dedicated to Dr. Franz Kummer on the Occasion of his 60th Birthday

ABSTRACT

It is an interesting exercise in materials science to explore simple rules relating the electronic properties of ternary systems to those of their binary constituents. In the present work, we have investigated the electronic structures of the large band gap gallates MGa_2O_4 (M=Mg, Ca, Ba and Zn) and the corresponding binary oxides MO and Ga_2O_3. Using first-principles band structure methods, we find that the metal atoms in MO control the width of the O 2p-like valence band and the size of the optical band gap. Covalent metal-oxygen bonding is much more pronounced in Ga_2O_3 and leads to characteristic structure in the valence band density of states. These basic features are retained in the ternary compounds where the covalent admixture to the chemical bond is largest between Ga and O, and the transitions across the band gap involve the Ga_2O_3 sublattice.

INTRODUCTION

There has been resurgence of interest in gallates, particularly zinc gallate, for application in thin film electro luminescent devices (TFEL), vacuum fluorescent displays (VFD), field emission display (FED) utilizing low-voltage cathode luminescence [1]. Gallates in M_2O-Ga_2O_3 and MO-Ga_2O_3 systems activated by divalent manganese was first investigated by Hoffman and Brown [2]. Magnesium gallate activated by manganese was used for a while as a green phosphor in specialty lamps. Recently zinc gallate has gained much attention as a blue emitter and manganese activated zinc gallate as a green emitter for VFDs and TFEL devices [1].

Understanding the electronic properties of the ternary oxides like $MgGa_2O_4$, $ZnGa_2O_3$ and $CaGa_2O_4$ from those of their binary building blocks CaO, MgO, ZnO and Ga_2O_3 is of importance from the perspective of materials design for specific application. This issue has already been the subject of our previous studies on a class of ternary oxides containing anionic groups with strong intra-atomic covalent bonding [3-5]. There we showed that the band gap transitions in the ternary compounds do not necessarily involve the highest occupied molecular orbitals (HOMO) and the lowest unoccupied molecular orbitals (LUMO) of the anionic groups.

In the present work, we report results from electronic structure calculations of the ternary gallates MGa_2O_4 (M=Mg, Ca, Ba and Zn) and their binary building blocks, MO and Ga_2O_3. In particular, we investigate how the HOMO-LUMO transitions change on going from the binary compounds MO and Ga_2O_3 to the ternary compounds. A systematic understanding of the correlations among the binary oxides and higher order oxides is helpful for predicting physical and chemical properties of more complex systems, and for engineering materials for specific purpose.

THEORY

The band structures of the compounds under study are computed using the augmented spherical wave (ASW) method [6] in a new scalar-relativistic implementation [7]. The calculations are based on density functional theory and the local density approximation. Since the ASW method uses the atomic sphere approximation with spherically symmetric potentials within Wigner-Seitz spheres of radii R_{AS} centered at the nuclei, we used empty spheres to fill the interatomic space in the open crystal structures associated with these oxides. These empty spheres can be considered as pseudo atoms without a nucleus, and are useful in modeling the correct shape of the crystal potential within large voids.

The ASW calculations were complemented by calculations using the new full potential (NFP) method [8,9]. Results from both approaches were found very similar. In both the ASW and NFP programs we used a minimal basis set (Mg (2s,2p), Ca (4s,4p,3d), Ga(4s,4p,3d), Zn(4s,4p,3d), Ba(6s,6p,5d) and O(2s,2p)) for the valence electrons comprising only one principal quantum number for each angular momentum state.

CRYSTAL STRUCTURES

MgO, BaO and CaO crystallize in the NaCl structure [10], and ZnO in the hexagonal wurtzite structure [11]. The β-form of gallium sesquioxide crystallizes in a monoclinic lattice with space group C2/m (No. 12) [12]. There are two kinds of Ga sites located in octahedral (Ga_2) and tetrahedral (Ga_1) sites. In contrast, oxygen atoms are arranged in a distorted close-packed structure. Metal-oxygen distances range from 1.80 to 1.85 Å in the tetrahedra and from 1.95 to 2.08 Å in the octahedra.

Several gallates crystallize in the (partially) inverse or normal spinel structure with two different cation sites, which are either tetrahedrally or octahedrally coordinated. $MgGa_2O_4$ is believed to have a partially inverse spinel structure [13,14]. However, in order to simplify the calculations, we have assumed a complete inverse spinel structure (space group Fd-3m, Nr. 227) using the structure data of Casado and Rasines [14] with Ga_1 on the tetrahedral and Mg and Ga_2 on the octahedral site.

The structure of $CaO\text{-}Ga_2O_3$ is more complicated than that of the corresponding Mg compound [15,16]. Beside many other phases, two stable $CaGa_2O_4$ phases exist, the orthorhombic o-$CaGa_2O_4$ phase and the monoclinic m-$CaGa_2O_4$ phase [16], which crystallize in silicate type of structure. In both the structures, one finds distorted GaO_4 tetrahedra, which form six-member rings. The two structures are distinguished by the orientation of the tetrahedra within the rings.

$ZnGa_2O_4$ crystallizes in the normal spinel structure [17] with Zn-O and Ga-O distances of 1.973 Å and 1.990 Å. Finally $BaGa_2O_4$ crystallizes in a hexagonal structure [18] with Ga in a tetrahedral coordination with d(Ga-O) = 1.726 – 1.819 Å and Ba in a 6+2 surrounding with d(Ba-O) = 2.845 – 3.100 Å.
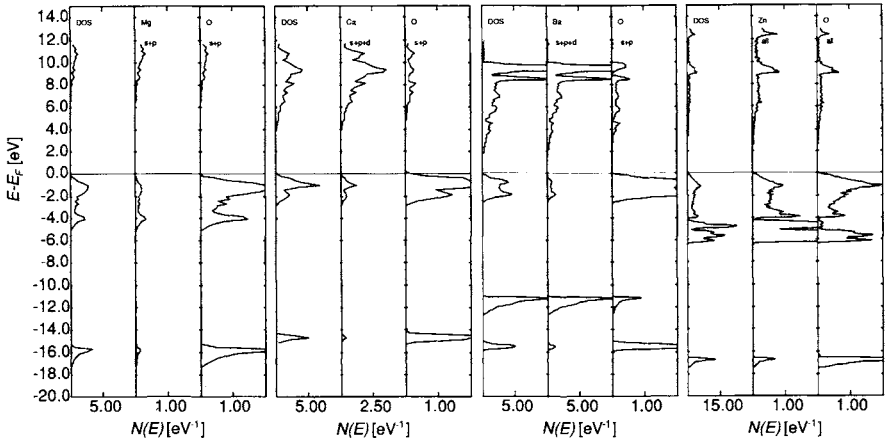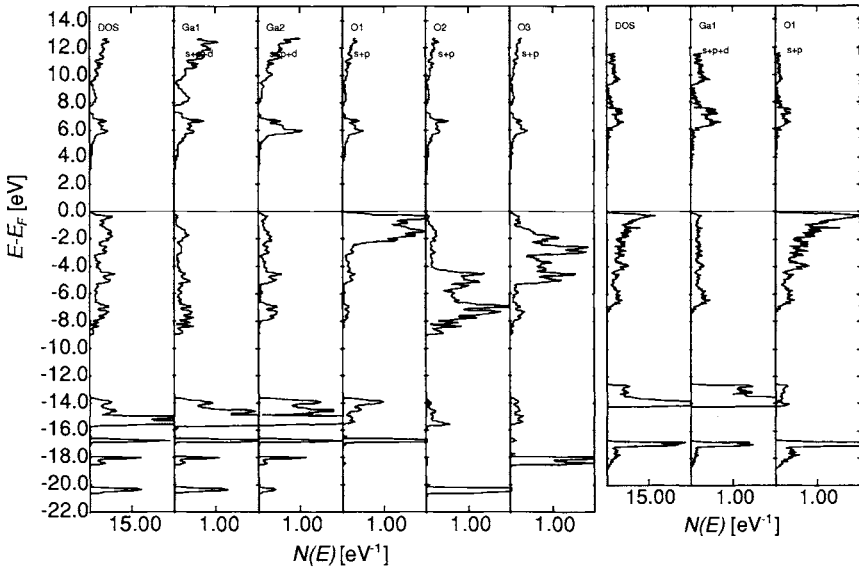
Figure 1: Density of States (DOS) and Partial Density of States (PDOS) of MgO, CaO, BaO and ZnO.

Figure 2: Density of States (DOS) and Partial Density of States (PDOS) of β-Ga₂O₃ (left) and α-Ga₂O₃ (right).

G1.2.3

ELECTRONIC STRUCTURE OF BINARY OXIDES

In Fig. 1, we display the partial densities of states (PDOS) of the binary oxides, MO. In all the plots, the zero of energy was fixed at the valence band maximum (E_F). The energy window was chosen to include low lying oxygen 2s states as well as mixed metal-oxygen states with predominant s-p components at high energies. For the IIA oxides, the valence bands result almost exclusively from the O 2p-like states. The small admixture of partial DOS coming from the cation and anion species indicates the ionic character of the bonding. While the charge density coming with the HOMO states is distinctly localized at the oxygen sites, the conduction states appear to be more delocalized.

Our findings for the group IIA oxides are contrasted by the results for ZnO. This material shows a considerably higher degree of covalency in the energy range from –4.0 eV to the valence band maximum, which is a consequence of the lower coordination coming with the wurtzite structure and the distinctly larger electronegativity of Zn compared to the IIA elements. In general, all our results are in good agreement with several previous studies on the electronic structure of these binary oxides (MgO [19], CaO [20], BaO [21], ZnO [22]).

The DOS for β-Ga_2O_3 and for the trigonal structure (α-Ga_2O_3) are displayed in Fig. 2. As we will see below, taking both structures into consideration allows to discuss the differences arising from the non-equivalent atomic sites in the β-phase. For both phases, we observe low lying oxygen 2s states at –17.0 eV and high lying mixed sp states above the optical band gap with larger contributions from the 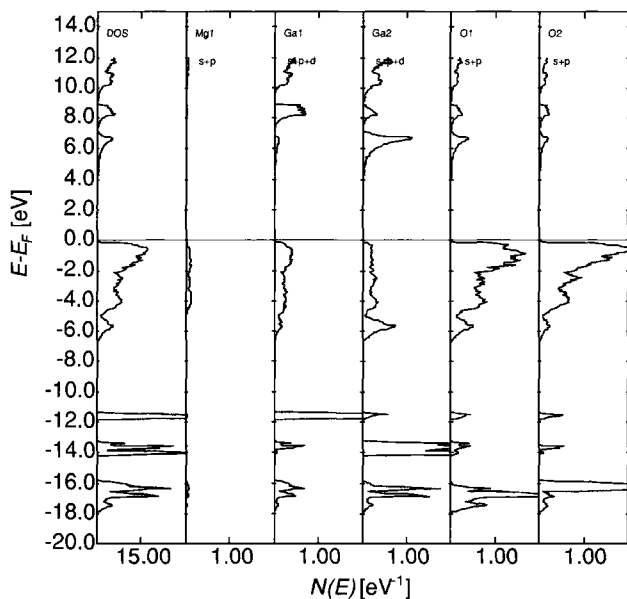metal states. In the energy range between –16.0 to –12.0 eV, the Ga 3d states give rise to a high partial DOS. Finally, the valence band for the lower valence states is made from similar contributions from the oxygen 2p and the metal states this indicating a large covalent character of these metal-oxygen states. It causes a considerable broadening of the valence band as compared to the binary oxides discussed above. However, the large valence band width in Ga_2O_3 results to a considerable degree from the diversity of metal and oxygen sites, which leads to a variety of metal-oxygen distances and coordinations. This situation leads, in particular, to the differences in oxygen

Figure 3: Density of States (DOS) and Partial Density of States (PDOS) of $MgGa_2O_4$.

partial DOS in β-Ga_2O_3, where O_1 and O_2 dominate in the upper and lower valence band region, respectively.

ELECTRONIC STRUCTURE OF GALLATES

The electronic structures of the gallates MGa_2O_4 may be essentially regarded as a superposition of the electronic states of the binary building blocks MO and Ga_2O_3, which we outlined in the previous section. While the main features apparently can be attributed to gallium sesquioxide, the change of the group II metal causes slight but distinct differences in the series MGa_2O_4. They trace back to the different spacings induced by the different sizes of the metal atoms and are rather independent from the details of the crystal structures. As it turns out, the optical properties and the character of the conduction band of the gallates can be predicted by the relative size of the band gaps of MO and Ga_2O_3. The partner with the smaller optical band gap eventually determines the optical band gap of the gallates.

In Fig. 3 we show the DOS of $MgGa_2O_4$. The O 2s and the Ga 3d like states are located below -10.0 eV. Because of the different sites of Ga, the position of the corresponding 3d like states differ by about 2.0 eV and are found at about -14.0 and -12.0 eV. Above these states we find the O 2p like states. The width of these bands of about 6.0 eV is slightly smaller than in Ga_2O_3. As expected from MgO the magnesium contribution in this energy range is very small indicating again a predominantly Mg-O ionic bonding. In contrast Ga-O bonding shows some covalent character. The lower conduction band states are very similar to those of Ga_2O_3. The amplitudes of these states are concentrated at O and Ga whereas we find almost no contribution of Mg. As mentioned above this finding is because the optical band gap of MgO is about 3.0 eV larger than that of Ga_2O_3.

Apart from the fact that the crystal structure of $CaGa_2O_4$ is more complicated, the gross features of its electronic structure are similar to those of $MgGa_2O_4$. However due to the higher number of non-equivalent sites, the DOS shows a large number of peaks. The situation is similar in $BaGa_2O_4$. The ordering of the partial DOS appears to be a superposition of the PDOS of the corresponding binary compounds. The band structure of both, $CaGa_2O_4$ and $BaGa_2O_4$, will be published elsewhere.

Finally, we display in Fig. 4 the partial DOS of $ZnGa_2O_4$. Since ZnO has a smaller optical band gap than Ga_2O_3 and the electronegativities of Ga and Zn are almost the same, the conduction band comprises similar contributions from all atoms. However, differences from the other three
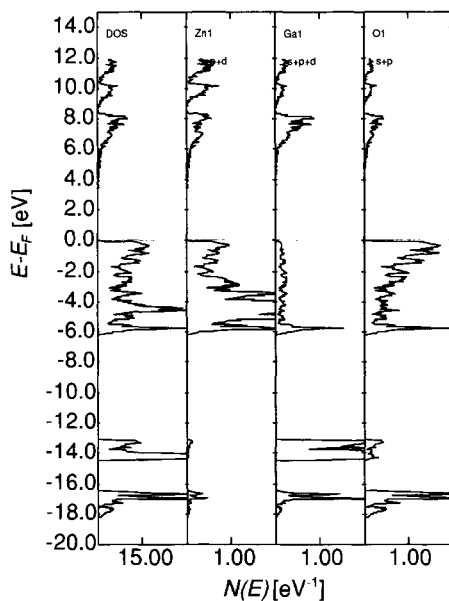

Figure 4: Density of States (DOS) and Partial Density of States (PDOS) of $ZnGa_2O_4$

G1.2.5

gallates stem essentially from the composition of the valence bands, which are dominated by the Zn 3d states. Only in the near gap region these states are superseded by the O 2p states. As a consequence, the charge density is not concentrated in the Ga_2O_3 sublattice but distributed over all three kinds of atoms.

CONCLUSION

In this report, we have discussed the electronic properties of the group II gallates MGa_2O_4 and related them to the binary building blocks MO and Ga_2O_3. The electronic structures of the ternaries arise from superposition of the electronic states of the respective binary partners. The nature of the chemical bond and the HOMO-LUMO transitions can be roughly predicted from the electronic properties of the binary counterparts.

REFERENCES

1. T. Minami, S. Takata, Y. Kuroi, T. Maeno, Soc. Inf. Dis. Sym. Digest **26**, 724 (1995), see references therein.
2. C.W.W. Hoffman, J.J. Brown, J. Inorg. Nucl. Chem. **30**, 63 (1968).
3. P.C. Schmidt, J. Sticht, V. Eyert, K.C. Mishra, Mat. Res. Soc. Symp. Proc. **560**, 323 (1999)
4. K.C. Mishra, B.G. DeBoer, P.C. Schmidt, I. Osterloh, M. Stephan, V. Eyert, K.H. Johnson, Ber. Bunsenges. Phys. Chem. **102**, 1772 (1998).
5. K. C. Mishra, I. Osterloh, H. Anton, B. Hannebauer, P. C. Schmidt, K. H. Johnson, J. Mater. Res. **12**, 2183 (1997).
6. A.R. Williams, J. Kübler, C.D. Gelatt Jr., Phys. Rev. B **19**, 6094 (1979).
7. V. Eyert, Int. J. Quant. Chem. **77**, 1007 (2000).
8. M. Methfessel, NFP Manual, IHP, Frankfurt (Oder) (1997).
9. E. Bott, M. Methfessel, W. Krabs, P.C. Schmidt, J. Math. Phys. **39**, 1 (1998).
10. W. Gerlach, Z. Phys. **9**, 184 (1922).
11. J. Albertsoon, S.C. Abrahams, A. Kvick, Acta Cryst. B **39**, 34 (1989).
12. S. Geller, J. Solid State Chem. **20**, 209 (1977).
13. T.F.W. Barth, E.Z. Pasnjak, Kristallografiya **82**, 325 (1932); F. Machatschki, Kristallografiya **82**, 348 (1932); H. Schmalzried, Z. Phys. Chem. **28**, 203 (1961); J.E. Weidenborner, N.R. Stemple Y. Okaya, Acta Crystallogr. **20**, 761 (1966).
14. P.G. Casado, I. Rasines, Z. Kristallogr. **160**, 33 (1982).
15. H.J. Deiseroth, H.K. Müller-Buschbaum, Z. anorg. Chem. **387**, 154 (1972); H.J. Deiseroth, H.K. Müller-Buschbaum, Z. anorg. Chem. **396**, 157 (1973); J. Jevaratham, F.P. Glasser, J. Amer. Ceram. Soc. **44**, 563 (1961); J. Jevaratham, F.P. Glasser, L.S. Dent Glasser, Z. Kristallogr. **118**, 257 (1963).
16. S. Ito, S. Banno, T. Kawano, K. Suzuki, Mat. Res. Bull. **16**, 313 (1981).
17. M. Wendschuh-Josties, H.St.C. O'Neill, K. Bente, G. Brey, Neues Jahrbuch f. Mineralogie **6**, 273 (1950).
18. H.J. Deiseroth, H.K. Müller-Buschbaum, J. Inorg. Nucl. Chem **35**, 3177 (1973).
19. Q.S. Wang, N.A.W. Holzwarth, Phys. Rev. B **41**, 3211 (1990).
20. R. Pandey, J.E. Jaffe, A.B. Kunz, Phys. Rev. B **43**, 9228 (1991).
21. M. Springborg, O.E. Taurian, J. Phys. C **19**, 6347 (1986).
22. W.F. Brinckmann, T.M. Rice, B. Bill, Phys. Rev. **8**, 1570 (1973).

ADVANCES IN THE DEVELOPMENT OF QUANTUM SPLITTING PHOSPHORS

A.A. Setlur[1], H.A. Comanzo[1], A.M. Srivastava[1], W.W. Beers[2], W. Jia[3], S. Huang[4], L. Lu[4], X. Wang[4], and W.M. Yen[4]
[1]GE Corporate Research and Development, Niskayuna, NY 12309
[2]GE Lighting, Cleveland, OH 44110
[3]Department of Physics and Astronomy, University of Puerto Rico, Mayaguez, PR 00681
[4]Department of Physics and Astronomy, University of Georgia, Athens, GA 30602

ABSTRACT

Quantum splitting phosphors (QSPs) are phosphors that could convert VUV radiation into more than one visible photon. These phosphors have the potential to improve the efficacy of current Hg fluorescent lamps and/or Xe lamps by reducing the Stokes shift energy loss after VUV excitation (λ_{exc}=185 nm for Hg lamps or 147 nm and 172 nm for Xe lamps provided the emission color of the phosphor matches the eye sensitivity. The current technology in QSPs and their potential limitations will be discussed in this paper. At GE-CRD, we have discovered and developed QSPs that meet the requirements for use in current Hg based fluorescent lamps. The steady state and time resolved optical properties of one of these phosphors, $SrAl_{12}O_{19}:Pr^{3+},Mg^{2+}$, has been measured to estimate the maximum quantum efficiency and onset of concentration quenching in this phosphor. The maximum quantum efficiency for $SrAl_{12}O_{19}:Pr^{3+},Mg^{2+}$ has been calculated to be ~125-135% for 185 nm excitation with an upper bound on the Pr^{3+} doping level of ~1%.

INTRODUCTION

Phosphors which have quantum efficiencies for visible light greater than unity are well known for cathode ray or x-ray excitation. However, the efficiency of phosphors that convert ultraviolet (UV) or vacuum ultraviolet (VUV) light into visible light is typically less than unity. If phosphors are developed which emit more than one photon for each incident UV or VUV photon absorbed, a quantum splitting phosphor (QSP), this could significantly improve the efficacy of current Hg or Xe based fluorescent lamps. The current focus of QSP research is develop visible quantum splitting phosphors to minimize energy loss upon VUV excitation, either from the 185 nm line from Hg lamps or the 172 nm/147 nm lines from Xe lamps.

One potential route to developing QSPs is to use energy transfer and cross-relaxation between various rare earth ions for the emission of two visible photons after VUV excitation. This has been clearly demonstrated in $LiGdF_4:Eu^{3+}$ which potentially has a quantum efficiency of 190% upon excitation into the ^6G_J levels of Gd^{3+} at ~200 nm (Figure 1) [1]. After VUV excitation, the $^6G_J \rightarrow {}^6P_J$ transition is resonant with the $^7F_1 \rightarrow {}^5D_0$ transition, leading to cross-relaxation and energy transfer to a Eu^{3+} ion. The Eu^{3+} ion then emits a orange-red photon, the first photon in this scheme. After the cross-relaxation between Gd^{3+} and Eu^{3+}, the ^6P_J level of Gd^{3+} is populated and this energy can then migrate along the Gd^{3+} sub-lattice until it reaches a Eu^{3+} ion, giving the second visible photon. Other quantum splitting schemes involving Er^{3+}-Gd^{3+}-Tb^{3+} in $LiGdF_4$ also have been demonstrated [2], but their efficiency has been estimated to be less than unity.
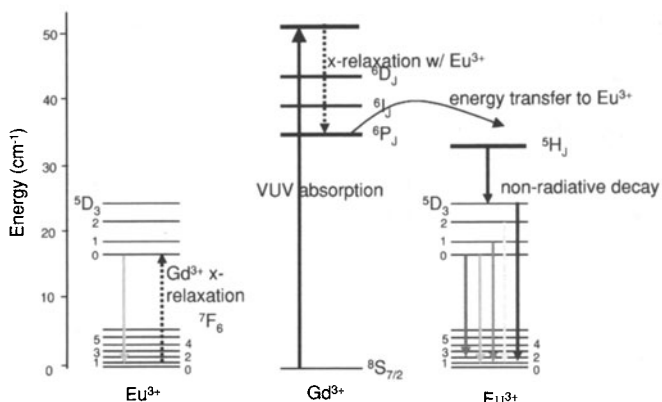
Figure 1. Schematic of quantum splitting process in LiGdF$_4$:Eu^{3+} (drawn from Ref. 1)

Another potential set of quantum splitting phosphors are based upon Pr^{3+} doped hosts [3]. The energy levels of Pr^{3+} are such that two visible photons can be emitted after excitation with one VUV photon (Figure 2), a quantum splitting process. This process occurs by Pr^{3+} absorbing VUV radiation through the allowed 4f→5d transition, non-radiative decay into the $^1S_0$ state at ~46500 cm^{-1}, emission to the $^1I_6$ level (405 nm radiation), non-radiative decay into the $^3P_0$ state, and $^3P_0$ emission (480-700 nm). This process requires the onset of the allowed 4f^2→4f5d absorption transition to be at high energy and above the $^1S_0$ state. If the 4f^2→4f5d absorption bands are below the $^1S_0$ state, the emission after VUV excitation will be either UV 4f5d→4f^2 emission bands [4] or $^3P_0$ or $^1D_2$ emission which can be directly fed by the 4f5d band [5]. In either case, the quantum efficiency of these phosphors can never exceed 100%.
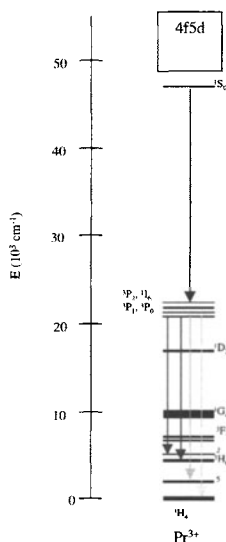

Figure 2. Schematic of the Pr^{3+} quantum splitting process. Note that the 4f5d band has to be above the $^1S_0$ level for quantum splitting to occur.

G1.6.2